

COARSE GRAINED LIOUVILLE DYNAMICS OF PIECEWISE LINEAR DISCONTINUOUS MAPS

M.E.Spina ^{a*} and M. Saraceno ^{a,b†}

^a *Dto. de Física, Comisión Nacional de Energía Atómica. Libertador 8250 (1429), Buenos Aires, Argentina.*

^b *Escuela de Ciencia y Tecnología, Universidad Nacional de San Martín. Alem 3901 (B1653HIM), Villa Ballester, Provincia de Buenos Aires, Argentina.*

(Dated: November 21, 2018)

We compute the spectrum of the classical and quantum mechanical coarse-grained propagators for a piecewise linear discontinuous map. We analyze the quantum - classical correspondence and the evolution of the spectrum with increasing resolution. Our results are compared to the ones obtained for a mixed system.

PACS numbers: 05.45.Mt

In this work we consider systems with a highly complex regular dynamics exhibiting, as in the chaotic case, an endless hierarchy of phase space structures. Examples of such dynamics are found in polygonal billiards on a surface with spherical curvature [1] and also in a class of maps introduced in [2, 3] that can be characterized as discontinuous piecewise linear. Typical phase space portraits of such maps are shown in Fig. (1). An infinite number of chains of elliptic islands pack the phase space. In the center of each island sits a stable periodic orbit of arbitrarily long period surrounded by a family of nested invariant curves which correspond to open orbits having an infinite but periodic sequence with the same period. The motion inside each island is regular. Their size decreases as the period increases and phase space takes a fractal structure. The boundary of the islands constitute the unstable set which is the infinite iteration of the discontinuity. The motion in these systems is non chaotic but highly irregular. In the case of the billiards this peculiar phase space is a consequence of the focusing mechanism on the sphere, while in the second case it is due to the discontinuity of the map.

The corresponding quantum mechanical systems have been investigated in both examples. For the billiards it was shown [4] that the quantum energy spectra follow a non universal intermediate statistics that can be understood in reference to the classical phase space plot, but no quantitative classical-quantum mechanical correspondence was derived. In [3] the semiclassical regime of a piecewise linear map was explored using Gutzwiller's method of periodic orbit quantization. However, as pointed out by the authors, great difficulties arose in their semiclassical approximation when describing the eigenstates not supported by stable periodic orbits. The relative failure of Gutzwiller's approach was attributed to the ellipticity of the dynamics of the map.

In the present contribution we attempt a different approach. We consider the discontinuous mapping introduced in [3] from the point of view of the spectral properties of the Liouville dynamics and study both the classical and the quantum Liouvillian at limited phase space resolution. The motivation is to compare the results to those well known that apply to chaotic or mixed systems [5, 6].

In pure hyperbolic systems the asymptotic decay of classical correlation functions is exponential and the decay rates can be rigorously obtained from the Ruelle-Pollicott (RP) resonances [7]. To study the long time behavior of general chaotic and mixed systems, which are beyond the validity of the RP theorem, non rigorous methods have been developed to compute the resonances of the Frobenius-Perron(FP)propagator. All these approaches are based on a coarse grained Liouville dynamics of the density function in the limit of zero coarse graining [8]. In [9] the blurring of phase space structures is implemented by adding a diffusive noise in the Liouville equation, which results in a coarse graining of the FP propagator and the limit of vanishing noise is finally considered . An alternative method developed in [5, 6] uses a truncation of the infinite unitary FP operator to a finite dimension N in a basis of functions ordered by increasing resolution. The eigenvalues of this non unitary $N \times N$ operator are calculated and the the limit $N \rightarrow \infty$ is taken. Since noisy propagation restores the quantum-classical correspondence, which is otherwise lost in short time scales, the computation of RP resonances for chaotic systems is a powerful tool to explore the link between classical and quantum mechanical dynamics and to look for the emergence of chaotic signatures in the quantum mechanical system.

In the present work we compute the spectrum of the classical coarse grained FP and quantum (Husimi) propagator for the discontinuous map on the sphere presented in [3], using the truncation method of [5, 6]. We follow closely the procedure that Haake and collaborators developed to study a system with mixed dynamics: the kicked top. We show that for low resolution classical and quantum mechanical propagators coincide, although the convergence is slow. We study the behavior of the eigenvalues and eigenfunctions of the truncated propagator with increasing resolution and compare our results to the ones obtained for a map with a mixed phase space [5].

The area preserving map considered in [3] acts on the angular momentum vector $\hat{J} = (J_x, J_y, J_z) = j (\sin \theta \cos \phi, \sin \theta \sin \phi, \cos \theta)$ of fixed length j . The corresponding phase space is the sphere, and $\cos \theta$ and ϕ the canonical variables. It has the form:

$$M = R_z(\omega) |R_x(\mu)| \quad (1)$$

that can also be rewritten as:

$$M = R_z(\omega) R_y(-\pi/2) |R_z(\mu)| R_y(\pi/2) \quad (2)$$

where $|R_i(\mu)|$ denotes a rotation around the J_i axis, of angle $\mu \text{ sign } J_i$. Under the action of this map the points on the sphere with $J_x < 0$ rotate in μ while those with $J_x > 0$ in $-\mu$ around the J_x axis. The whole sphere rotates then in ω around the J_z axis. That is, at each step, every point rotates linearly except for the ones on the great circle $J_x = 0$ where the map becomes singular. The unstable set is constituted by all the images and preimages of this great circle. This is evidenced in the phase space portrait. The bounds of one island of each chain are tangent to the instability line $\phi = \pi/2, 3\pi/2$.

The evolution of the phase space density ρ of the system is given by:

$$\rho_{n+1}(\cos \theta, \phi) = \mathcal{P} \rho_n(\cos \theta, \phi) \quad (3)$$

where \mathcal{P} is the FP propagator that is related to the invertible map (1) by:

$$\mathcal{P} \rho(\cos \theta, \phi) = \rho(M^{-1}(\cos \theta, \phi)) \quad (4)$$

Eq.(3) results from the formal integration of the Liouville equation:

$$\partial_t \rho = \mathcal{L} \rho \quad (5)$$

Defining the Liouvillians corresponding to each rotation in eq.(2), the FP operator corresponding to this map reads $\mathcal{P} = \exp[\mathcal{L}_{R_z(\omega)}] \exp[\mathcal{L}_{R_y(-\pi/2)}] \exp[\mathcal{L}_{|R_z(\mu)|}] \exp[\mathcal{L}_{R_y(\pi/2)}]$.

The matrix elements of \mathcal{P} can be computed in the basis of the spherical harmonics $Y_{lm}(\theta, \phi)$, which span the space of phase space functions on the sphere and are ordered according to increasing resolution by index l .

It can be easily shown that:

$$(\exp[\mathcal{L}_{R_z(\omega)}])_{lm, l' m'} = \delta_{l, l'} \delta_{m, m'} \exp[-im\omega] \quad (6)$$

$$(\exp[\mathcal{L}_{R_y(\omega)}])_{lm, l' m'} = \delta_{l, l'} d_{m, m'}^l(\omega) \quad (7)$$

$$\begin{aligned} & (\exp[\mathcal{L}_{|R_z(\mu)|}])_{lm, l' m'} = \\ & \int_0^{2\pi} d\phi \left\{ \int_{-1}^0 d \cos \theta Y_{lm}^*(\theta, \phi) Y_{l' m'}(\theta, \phi - \mu) + \int_0^1 d \cos \theta Y_{lm}^*(\theta, \phi) Y_{l' m'}(\theta, \phi + \mu) \right\} \\ & = \delta_{m, m'} \begin{cases} \cos \mu & \text{for } l = l' \\ 0 & \text{for even } l - l' \\ i/2 \sin m\mu \int_{-1}^0 d \cos \theta P_{l, m}(\cos \theta) P_{l', m'}(\cos \theta) & \text{for odd } l - l' \end{cases} \quad (8) \end{aligned}$$

where $d_{m, m'}^l(\omega)$ are the Wigner's d-matrix and $P_{l, m}(\cos \theta)$ the Legendre functions. The last matrix element, which can be computed analytically, couples subspaces with different values of l . Therefore, a truncation of \mathcal{P} up to a finite l_{max} leads to a non unitary matrix.

The quantum version of the map in the Hilbert space of the wave functions spanned by the $(2j + 1)$ eigenvectors of \hat{J}_z , $|jm\rangle$, is given by the Floquet operator:

$$\begin{aligned}\hat{F} &= \exp[-i\omega\hat{J}_z] \exp[-i\mu|\hat{J}_x|] \\ &= \exp[-i\omega\hat{J}_z] \exp[-i\pi/2\hat{J}_y] \exp[-i\mu|J_z|] \exp[i\pi/2\hat{J}_y]\end{aligned}\quad (9)$$

where:

$$|\hat{J}_z| = \sum_{m=-j}^j |m| |jm\rangle$$

The density operator $\hat{\rho}$ is now represented by the corresponding Husimi function $Q_\rho(\theta, \phi) = \langle j\theta\phi|\hat{\rho}|j\theta\phi\rangle$ (that is, its diagonal matrix element in the basis of coherent states) and its time evolution is given by:

$$\partial_t Q_\rho = \mathcal{G} Q_\rho \quad (10)$$

The Husimi propagator $\exp[\mathcal{G}]$ is a unitary matrix of dimension $(2j + 1)^2$. As for the classical case their matrix elements $\exp[\mathcal{G}] = \exp[\mathcal{G}_{R_z(\omega)}] \exp[\mathcal{G}_{R_y(-\pi/2)}] \exp[\mathcal{G}_{|R_z(\mu)|}] \exp[\mathcal{G}_{R_y(\pi/2)}]$ will be calculated in the basis of the spherical harmonics.

As shown in [6] the Husimi propagator for rotations is identical to its classical counterpart. We are then left with the calculation of $\exp[\mathcal{G}_{|R_z(\mu)|}]_{lm, l'm'}$, whose spectral representation is:

$$\exp[\mathcal{G}_{|R_z(\mu)|}] = \sum_{m_1, m_2=-j}^j Q_{|jm_1\rangle\langle jm_2|} \exp[-i(\mu|m_1| - |m_2|)] P_{|jm_1\rangle\langle jm_2|} \quad (11)$$

where Q and P (the Q- and P-functions corresponding to $|jm_1\rangle\langle jm_2|$) are respectively the right-hand and left-hand eigenfunctions of $\exp[\mathcal{G}_{|R_z(\mu)|}]$ with eigenvalue $\exp[-i\mu(|m_1| - |m_2|)]$. To express the matrix elements of the propagator (11) in the basis of the spherical harmonics, we need to calculate the scalar products $\langle Y_{lm}|Q_{|jm_1\rangle\langle jm_2}| \rangle$ and $\langle Y_{lm}|P_{|jm_1\rangle\langle jm_2}| \rangle$ which are sums of Clebsch Gordan coefficients. We finally obtain:

$$\exp[\mathcal{G}_{|R_z(\mu)|}]_{lm, l'm'} = \delta_{m, m'} \frac{2l+1}{2j+1} \sum_{m_1=\max(-j+m, -j)}^{\min(j, j+m)} C_{j(m_1-m), lm}^{jm_1} C_{j(m_1-m), l'm}^{jm_1} \exp[-i\mu(|m_1| - |m_1 - m|)] \quad (12)$$

As in the classical case the matrix elements of the propagator are diagonal in m , but non diagonal in l .

We can easily show that when $\exp[\mathcal{G}]$ is truncated to a dimension $N = (l_{max} + 1)^2$ with $l_{max} \ll 2j$ it approaches its classical counterpart $\mathcal{P}^{(N)}$. In this limit the sum in eq.(12) can be approximated by:

$$\exp[\mathcal{G}_{|R_z(\mu)|}]_{lm, l'm'} \approx \delta_{m, m'} \frac{2l+1}{2j+1} [\exp[i\mu m] \sum_{m_1=-j}^0 C_{j(m_1-m), lm}^{jm_1} C_{j(m_1-m), l'm}^{jm_1} + \exp[-i\mu m] \sum_{m_1=1}^j C_{j(m_1-m), lm}^{jm_1} C_{j(m_1-m), l'm}^{jm_1}] \quad (13)$$

since $|m| \leq l_{max} \ll 2j$. Using then the asymptotic expression for $l \ll j$ of the Clebsch Gordan coefficients [10]:

$$C_{j(m_1-m), lm}^{jm_1} \rightarrow \sqrt{\frac{4\pi}{(2l+1)}} Y_{lm}(\theta, 0) \quad (14)$$

(where θ is the angle between \hat{j} and the z-axis) and approximating $\frac{1}{2j+1} \sum_{m_1=-j}^0$ by $\int_{-1}^0 d\cos\theta$ we recover eq.(8). Therefore the matrix elements of the quantum propagator given by eq.(12) coincide with their classical counterpart of eq.(8) for low resolution and in this limit it will be equivalent to study the spectrum of the FP or the Husimi propagator. However the convergence of the quantum mechanical propagator to the FP propagator is much slower than the one found for the kicked top in [6], where the quantum mechanical corrections were of the order of $l/2j + 1$. This can be appreciated when comparing the quantal spectra of Fig. 2, with $l_{max} = 20$ and different values of j , with the corresponding classical spectrum of Fig.4 a). The convergence gets worse as l_{max} increases, as shown in Fig. 3 which displays quantal spectra for $l_{max} = 40$ and different values of j (to be compared with Fig. 4 b)).

We now diagonalize the truncated FP operator $\mathcal{P}^{(N)}$, whose elements are given by eqs.(6,7,8) in the subspace spanned by $N = (l_{max} + 1)^2$ spherical harmonics with $0 \leq l \leq l_{max}$. This corresponds to a resolution of phase space structures of area $4\pi/((l_{max} + 1)^2)$. Two sets of parameters ω, μ are considered in the map eq.(1) with the corresponding phase portraits shown in Fig.1. In the first case (Case I, $\omega = \mu = \pi(\sqrt{5} - 1)$) few big elliptic islands are present, corresponding to orbits of low periodicity. In the second (Case II, $\omega = 1, \mu = 0.05$) the quasi tori surviving in correspondence to the integrable case ($\mu = 0$) are visible.

In Fig. 4 we display the eigenvalue spectrum of $\mathcal{P}^{(N)}$ corresponding to Case I for different values of l_{max} . For coarse resolution $l_{max} = 20$ most of the eigenvalues λ_i concentrate inside a ring corresponding to $0.9 \leq |\lambda_i| \leq 1$. As the resolution increases, the outer ring becomes narrower (for $l_{max} = 70, 0.95 \leq |\lambda_i| \leq 1$) and the fraction of the eigenvalues located in the inner disk decreases. In Case II, the situation is very much the same for $l_{max} = 70$, that is, there is a very high concentration of eigenvalues inside a narrow ring and a few values lying in the inner disk. However for low resolution $l_{max} = 20$ the distribution looks different: most of the eigenvalues lie close to the unit circle. Other spectra have been computed for different values of the map's parameters ω and μ , corresponding to different types of phase space portraits with more or less dominant islands. The characteristics of the spectra differ from case to case depending on the number of domains that can be resolved at each given resolution. This non universality was also remarked in [4] where the calculation of quantal spectra of triangular billiards on the sphere showed that the level distributions do not follow a universal statistics but can rather be understood in reference to the phase space portrait corresponding to each particular case. However the general features of spectra obtained with high resolution are the same in all cases. There is always a densely populated outer ring, corresponding to unimodular and almost unimodular eigenvalues, and a small fraction of the eigenvalues lying in the inner disk. The eigenvalues move about when increasing l_{max} and no 'frozen' eigenvalues can be individualized.

A better understanding of the spectrum is achieved by plotting the distributions of the N eigenvalues as a function of their modulus for different resolutions. As shown in Figs.6 (for Case I and II, and $l_{max} = 50, 60, 74$) we can distinguish three regions: a peak at $0.95 \leq |\lambda_i| \leq 1$, an intermediate domain corresponding to approximately $0.85 \leq |\lambda_i| \leq 0.95$ which looks very much the same for all resolutions and a small number of values with $|\lambda_i| \leq 0.85$. While the peak corresponding to $0.95 \leq |\lambda_i| \leq 1$ grows for increasing values of l_{max} , the number of states with $|\lambda_i| \leq 0.95$ remains fairly constant, so that the fraction of non unimodular eigenvalues decreases with increasing resolution. Moreover, the numerical results seem to imply in the intermediate region a relationship $n(|\lambda|) \sim |\lambda|^\alpha$ where the exponent α is independent of the resolution. At this stage we cannot interpret this observation. The eigenfunctions corresponding to these three regions are of different nature. Some examples are represented in Fig.7 for Case I and $l_{max} = 70$ and in Fig.8 for Case II and $l_{max} = 70$. Eigenfunctions with unimodular eigenvalue are shown in Fig. 7a) and Fig.8a): they are supported by the elliptic islands that can be resolved at the corresponding l_{max} . Eigenfunctions corresponding to quasi unimodular eigenvalues ($0.9 \leq |\lambda_i| \leq 0.95$) have the structure displayed in Fig.7b) and Fig.8b) . Their amplitude is evenly distributed over a large number of islands. Finally for $|\lambda_i| \leq 0.85$ the eigenfunctions are of the type shown in Fig.7c),d) and Fig.8c),d): they locate along the unstability line and along curves which are their first iterations by the map M .

On the basis of these numerical results we can describe the $\mathcal{P}^{(N)}$ spectrum, consisting of unimodular, almost unimodular and non unimodular eigenvalues, and its evolution with N as follows. Unimodular eigenvalues correspond to eigenfunctions which locate in the elliptic islands visible at the given resolution: when N grows more and more elliptic structures are resolved and their number increases. The group of almost unimodular eigenvalues correspond to eigenfunctions which are not fully localized yet and spread over several islands. The fact that their number remains approximately constant with N , showing a compensation between the migration of existing eigenvalues to the unit circle and the appearance of new ones, related to still unlocalized states, can be explained by the existence of an infinite hierarchy of phase space structures which are gradually resolved. Finally, we saw that eigenvalues with moduli $|\lambda_i| \leq 0.85$ correspond to eigenstates sharply localized on the unstability line. These states are present for any value of N . However, their number seems to be approximately constant, so that they will represent a vanishing fraction of the total spectrum in the limit $N \rightarrow \infty$.

As expected, the observed evolution of the $\mathcal{P}^{(N)}$ spectrum with N is different from the one obtained for the integrable system (corresponding to $\mu = 0$ in our map), where all eigenvalues migrate to the unit circle in the $N \rightarrow \infty$ limit and unitarity is recovered. The situation is also different from the one observed for chaotic systems, where $\mathcal{P}^{(N)}$ has an essential spectrum inside a circle of radius ($r > 0$) and a point spectrum inside a disk $r < |\lambda| < 1$, with some eigenvalues (that can be related to the RP resonances) persisting in their positions for increasing values of N [5]. In the system under study, non unimodular eigenvalues exist and can be interpreted, as in the chaotic case, as an effective dissipation due to the loss of probability to finer unresolved structures. However 'freezing' which in the case of chaotic dynamics is attributed to the self similarity in phase space, is not observed. Thus the 'resonances' will not be a characteristic of the classical system but rather will depend on the resolution. In addition, the fraction of non

unimodular eigenvalues vanishes in the limit $N \rightarrow \infty$, since it is related to the measure of the unstable set.

Summarizing, we computed the matrix elements of the FP operator $\mathcal{P}^{(N)}$ and of the quantum Husimi propagator for discontinuous piecewise linear systems and showed that they coincide in the limit of low resolution. We investigated the evolution of the spectra of the truncated propagator $\mathcal{P}^{(N)}$ with N . We observed significant differences with respect to the results obtained for systems with chaotic or mixed phase spaces, where this truncation procedure is used to get the RP resonances related to the decay rate of correlations. One is the absence in our case of stable eigenvalues persisting in their positions for $N \rightarrow \infty$. Another fundamental difference is the fact that the fraction of the non unimodular eigenvalues, present for all values of the resolution and corresponding to eigenfunctions localized on the instability line and their images, decreases for increasing values of the resolution. This can be taken as an indication of the zero measure of the unstable set.

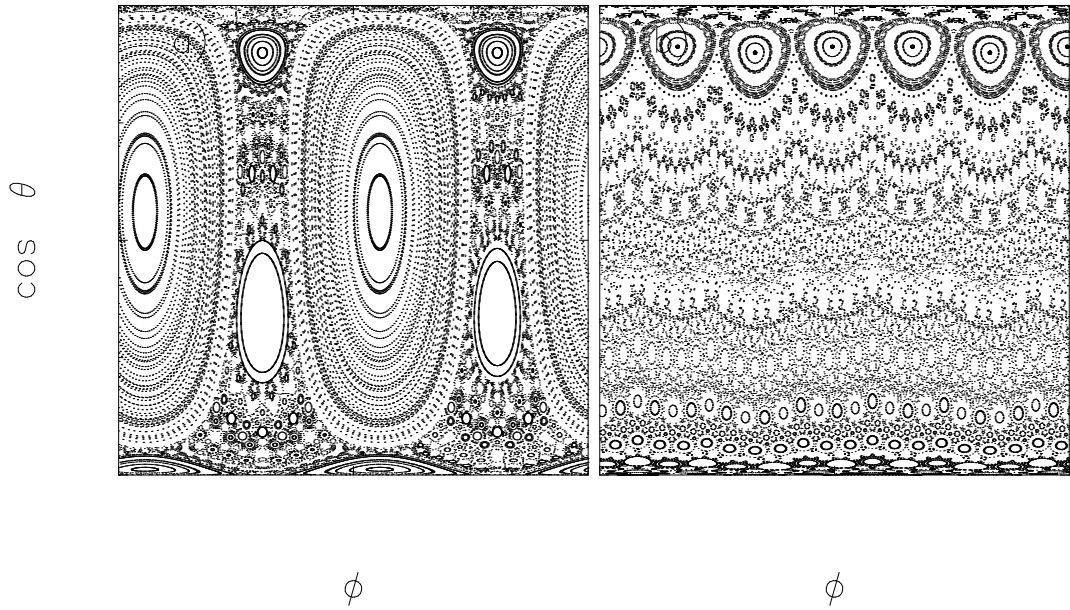


FIG. 1: Phase space portrait of map eq.(1) for a) $\omega = \mu = \pi(\sqrt{5} - 1)$ (Case I), b) $\omega = 1, \mu = 0.05$ (Case II).

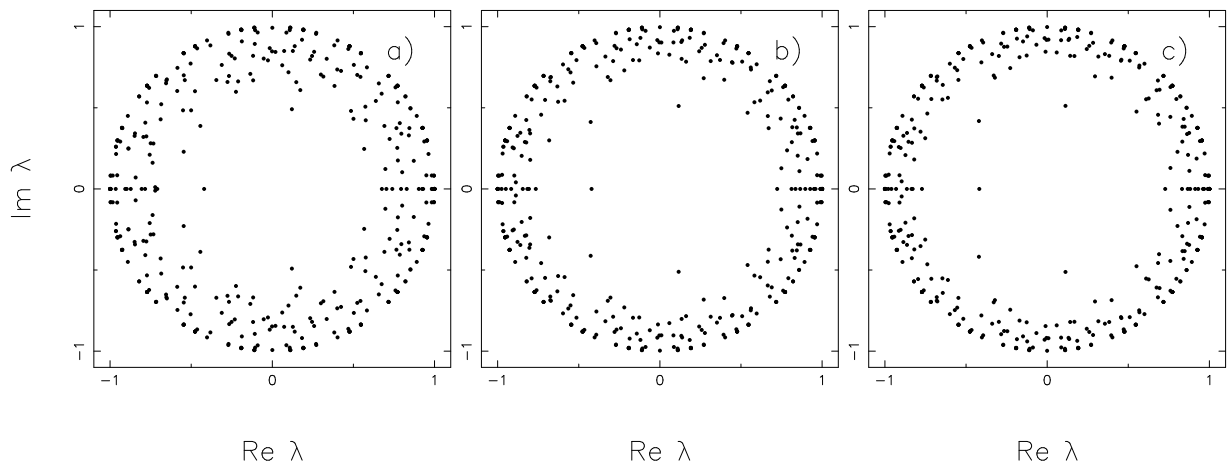


FIG. 2: Quantal spectrum (Case I) corresponding to $l_{max} = 20$ for $j=100, 200, 300$.

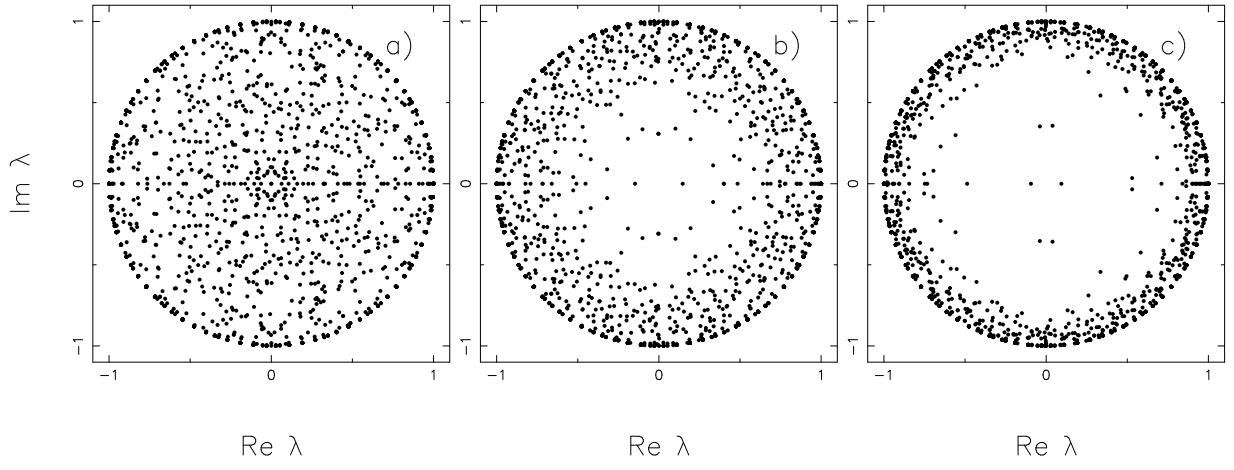


FIG. 3: Quantal spectrum (Case I) corresponding to $l_{max} = 40$ for $j = 100, 200, 700$.

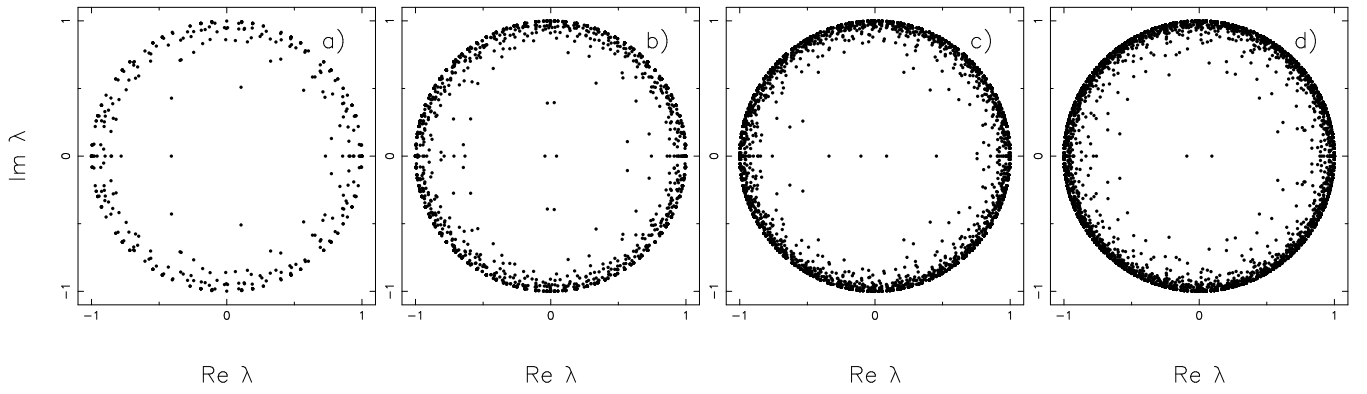


FIG. 4: Classical spectrum (Case I) for $l_{max} = 20, 40, 60, 70$.

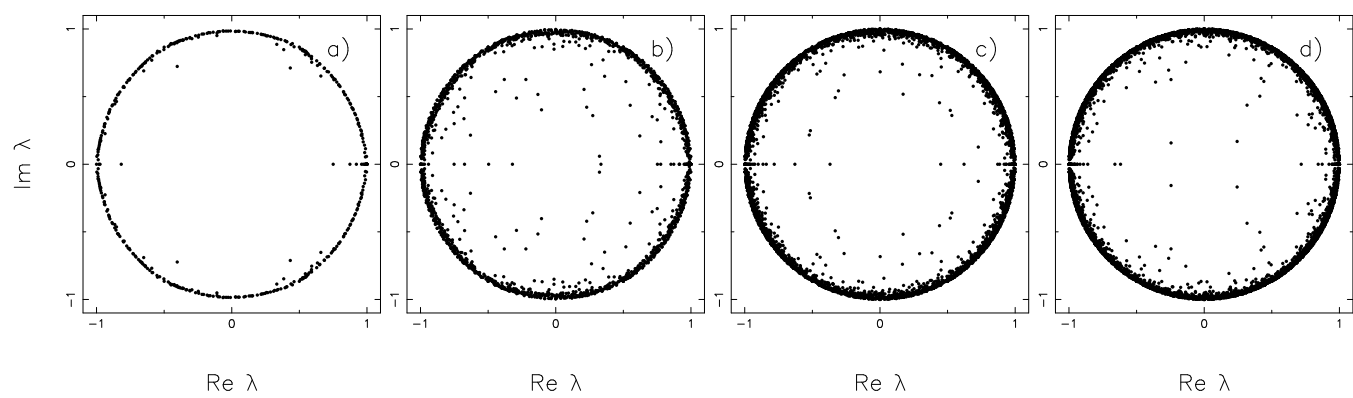


FIG. 5: Classical spectrum (Case II) for $l_{max} = 20, 40, 60, 70$.

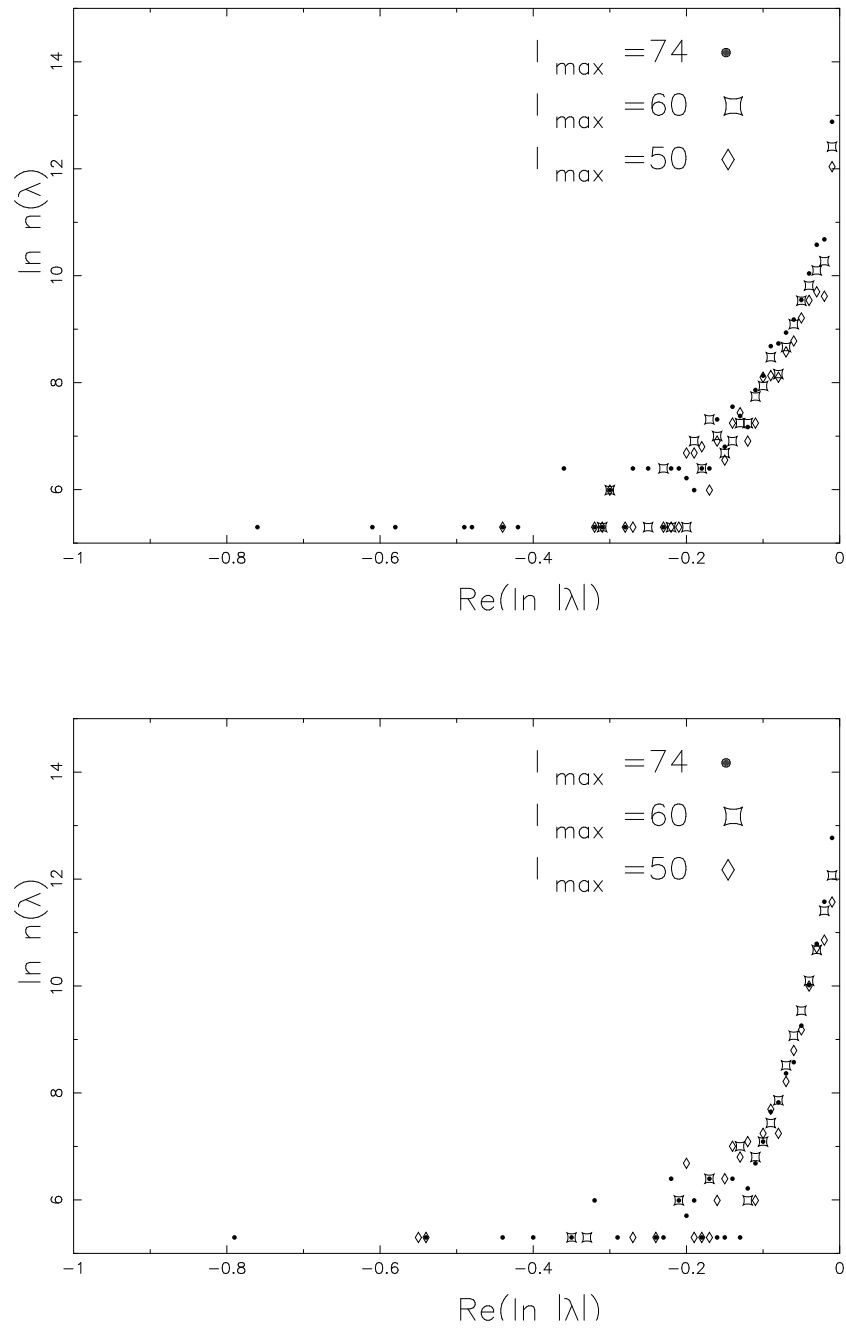


FIG. 6: Number of eigenvalues (in a logarithmic scale) as a function of $\ln|\lambda_i|$ for different values of l_{\max} in a) Case I and b) Case II.

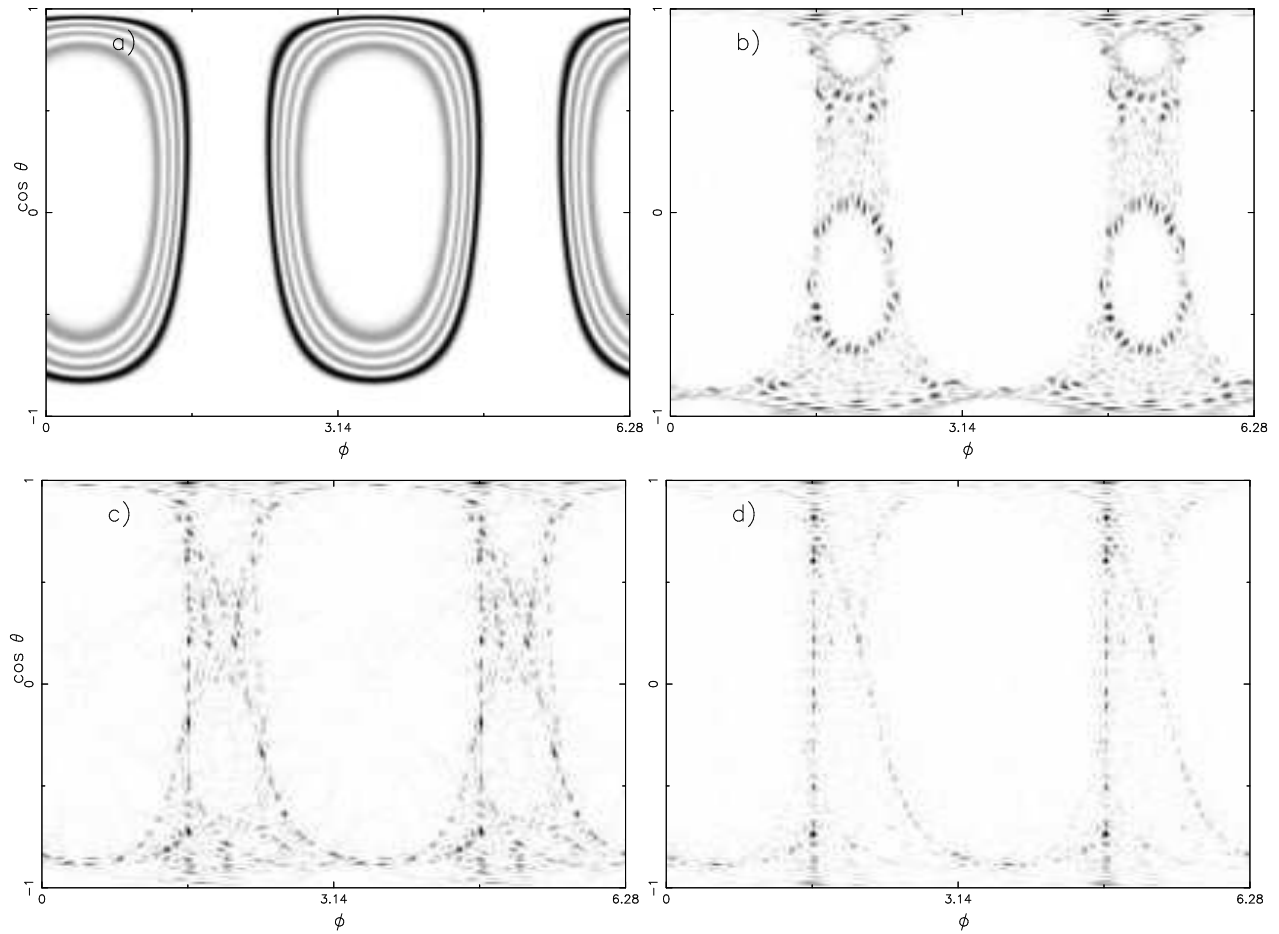


FIG. 7: Eigenfunctions of the classical propagator $\mathcal{P}^{(N)}$ (Case I , $l_{max} = 70$) corresponding to eigenvalues with a) $|\lambda| = 1$, b) $|\lambda| = 0.97$, c) $|\lambda| = 0.85$, d) $|\lambda| = 0.72$.

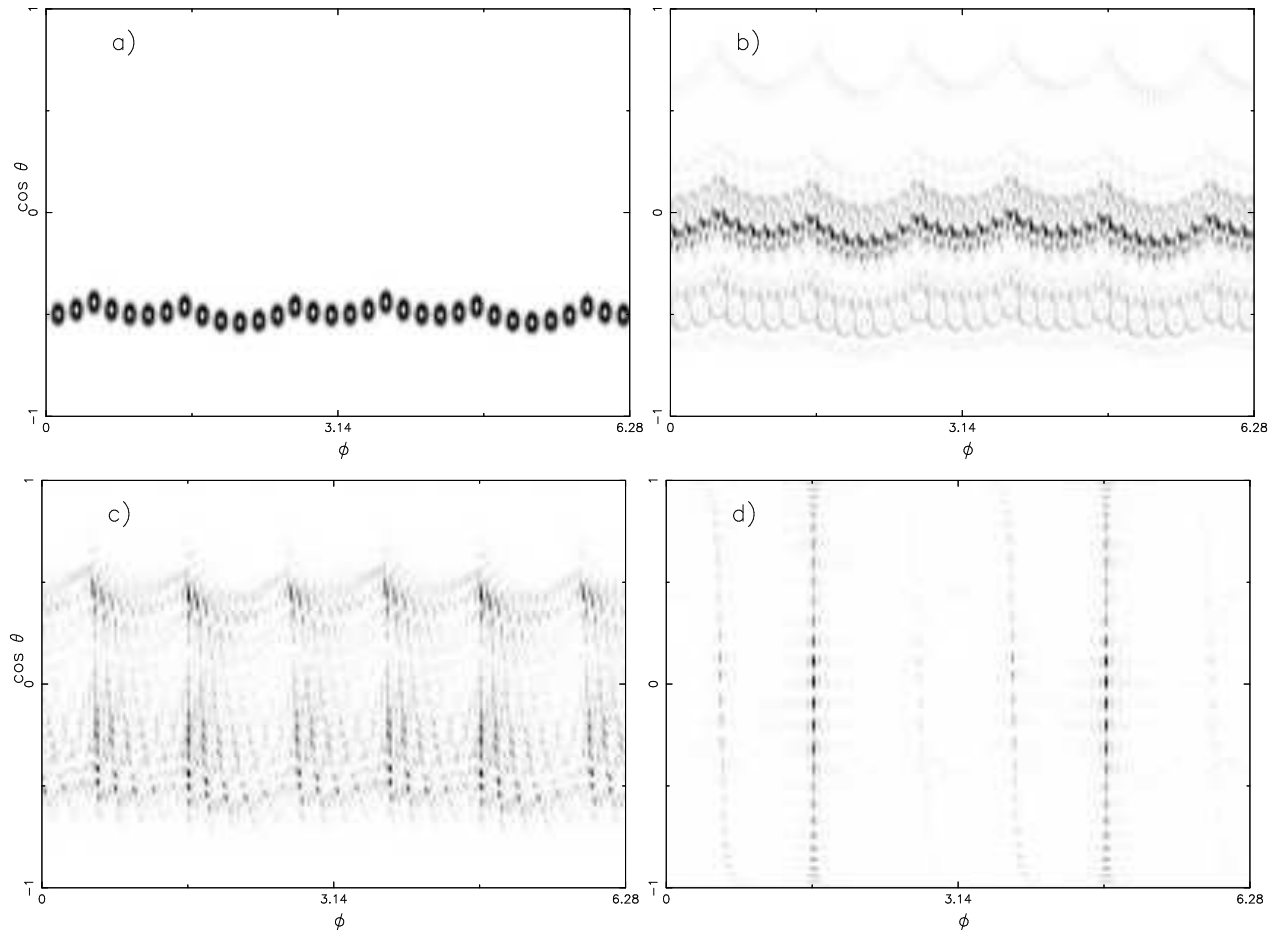


FIG. 8: Eigenfunctions of the classical propagator $\mathcal{P}^{(N)}$ (Case II , $l_{max} = 70$) corresponding to eigenvalues with a) $|\lambda| = 1$, b) $|\lambda| = 0.95$, c) $|\lambda| = 0.88$, d) $|\lambda| = 0.75$.

* Electronic address: spina@tandar.cnea.gov.ar

† Electronic address: saraceno@tandar.cnea.gov.ar

- [1] Spina M.E and Saraceno M. 1999 *J.Phys.A* **32** 7803
- [2] Scott A.J. , Holmes C.A. and Milburn G.J. 2001 *Physica D* **155** 34
- [3] Scott A.J. and Milburn G.J. 2001 *J.Phys.A* **34** 7541
- [4] Spina M.E. and Saraceno M. 2001 *J.Phys.A* **34** 2549
- [5] Weber J., Haake F. and Seba P. 2000 *Phys. Rev. Lett.* **85** 3620 ; Weber J., Haake F., Braun P., Manderfeld C. and Seba P. 2001 *J.Phys A* **34** 7195
- [6] Manderfeld C., Weber J. and Haake F. 2001 *J.Phys A* **34** 9893
- [7] Ruelle D. 1986 *Phys. Rev. Lett.* **56** 405
- [8] Fishman S. and Rahav S. 2002 *Lectures Notes in Physics: Dynamics of Dissipation*, (eds.Garbaczewski P. and Olkiewicz R., Springer-Verlag, Berlin)
- [9] García-Mata I., Saraceno M. 2004 *Phys.Rev. E* **69** 056211
- [10] Varshalovich D.A., Moskalev A.N. and Khersonskii V.K. 1988 *Quantum Theory of Angular Momentum* (World Scientific)